Quim. Nova, Vol. 29, No. 2, 223-229, 2006

Artigo

Cu AND Co EXCHANGED ZSM-5 ZEOLITES – ACTIVITY TOWARDS NO REDUCTION AND HYDROCARBON OXIDATION

Leandro Martins, Robson Pablo Sobradiel Peguin e Ernesto Antonio Urquieta-González*
Departamento de Engenharia Química, Universidade Federal de São Carlos, CP 676, 13560-970 São Carlos – SP

Recebido em 4/1/05; aceito em 29/6/05; publicado na web em 20/1/06

|Cu_x|[Si_yAl]-**MFI** and |Co_x|[Si_yAl]-**MFI** catalysts were prepared by ion exchange from |Na|[Si_yAl]-**MFI** zeolites (y = 12, 25 and 45). The activity of the catalysts was evaluated in the reduction of NO to N_2 in an oxidative atmosphere using propane or methane as reducing agents. The Cu catalysts were only active with propane and they presented higher activity than the Co-based catalysts, the latter being active with both hydrocarbons. H_2-TPR and DRS-UV/Vis data allowed correlation between the activity towards NO reduction and the presence of cationic charge-compensating species in the zeolite. It was also verified that the hydrocarbons are preferentially oxidised by O_2, a reaction that occurs simultaneously with their oxidation with NO.

Keywords: |Cu_x|[Si_yAl]-**MFI**, |Co_x|[Si_yAl]-**MFI**; NO reduction; propane oxidation.

INTRODUCTION

Environmental laws, which regulate the level of emission of nitrogen oxides (NO_x) and other primary pollutants into the atmosphere, are becoming more restrictive. Thus, a large number of studies that aim to improve the catalytic conversion of NO_x to N_2 by decomposition or reduction are being performed[1,2]. Special attention has been given to the selective catalytic reduction of NO with hydrocarbons (SCR-HC) under oxidative conditions, which is a potential solution for the treatment of exhaust gases that are generated by diesel engines or other combustion processes[3].

In such processes the use of transition metal exchanged zeolites, as selective catalysts, has been proposed. Since the initial study by Iwamoto and Hamada[4], which demonstrated that Cu exchanged ZSM-5 (|Cu_x|[Si_yAl]-**MFI**) are active catalysts for the SCR-HC, several types of this catalyst have been intensively studied. The possible species present in |Cu_x|[Si_yAl]-**MFI** type catalysts, generally identified by FTIR, H_2-TPR, EPR or EXAFS, are copper cations (Cu^{2+}), oxocations $(Cu\text{-}O\text{-}Cu)^{2+}$ or copper oxide (CuO)[5]. The presence of one particular species in the metal-exchanged zeolite depends on the exchanged metal content, on the pH value used during the ion exchange and on the atmosphere used during the subsequent thermal treatment. According to Gómez *et al.*[6], the cationic species Cu^{2+} and Cu^{+} in Cu-catalysts have an important role in the catalytic reduction of NO_x by hydrocarbons. Although these Cu based zeolitic catalysts show high activity for the SCR-HC from 400 to 800 ºC, they deactivate rapidly in an atmosphere which contains excess of water and/or sulphur oxides[7]. On the other hand, in contrast to Cu-based catalysts, zeolites containing Co-species have been demonstrated to be more promising due to their better catalytic performance under hydrothermal conditions[8].

In addition to the deactivation by water vapour of Cu and Co-exchanged ZSM-5 zeolites during the SCR-HC, it has also been pointed out that preferential direct hydrocarbon oxidation by O_2 rather than the desired reaction with NO can occur[2], such behaviour limiting their activity towards the SCR-HC and more intensely at temperatures higher than 450 ºC (Table 1, reactions 2 and 4)[9]. Although some water is formed in these reactions (lower than 0.6%, v/v), the amount present is not plausible to cause appreciable deactivation[7].

Table 1. Main reactions occurring during the SCR-HC

Number	Reaction	$-\Delta G_{298}$* / Kcal mol^{-1}
1	$2NO + C_3H_8 + 4O_2 \rightarrow N_2 + 3CO_2 + 4H_2O$	536.4
2	$C_3H_8 + 5O_2 \rightarrow 3CO_2 + 4H_2O$	495.0
3	$2NO + CH_4 + O_2 \rightarrow N_2 + CO_2 + 2H_2O$	232.6
4	$CH_4 + 2O_2 \rightarrow CO_2 + 2H_2O$	191.3

*Estimated from data available in reference 10.

In the discussed field, the present study aims to verify the activity of |Cu_x| and |Co_x|[Si_yAl]-**MFI** catalysts in the NO reduction, using methane or propane as reducing agents, and for the simultaneous hydrocarbon oxidation with O_2. The results obtained will be related to the metallic species formed during the preparation and activation of the catalysts.

EXPERIMENTAL PART

Preparation of the catalysts

The precursor |Na|[Si_yAl]-**MFI** zeolites (where y = 12, 25, and 45 represent the Si/Al ratio in the solid and **MFI** the ZSM-5 structure)[11,12] were synthesised as described elsewhere[13]. The synthesis was achieved using *n*-butylamine ($C_4H_9NH_2$ 98%, Riedel-de-Häen) as organic template and sodium trisilicate ($Na_2Si_3O_7 \times H_2O$ 99%, Aldrich) and aluminium sulphate hydrate ($Al_2SO_4 \times 14–18H_2O$ 99%, Reagen) as silica and aluminium sources, respectively. The zeolites were crystallised under autogenous pressure in static conditions at 170 ºC. After the synthesis, the *n*-butylamine occluded in the microporous of the zeolite was removed by calcination at 520 ºC for 16 h, using a heating rate of 1 ºC min^{-1} and an air flow of 40 mL min^{-1} $g_{catalyst}^{-1}$. The |Cu_x| and |Co_x|[Si_yAl]-**MFI** catalysts (where x represents the metal/aluminium ratio) were obtained from the precursor |Na|-zeolite by ion exchange in aqueous solutions of 0.015 mol L^{-1} of copper (II) acetate ($Cu(O\text{-}CO\text{-}CH_3)_2$ 99%, Merck) or of cobalt (II) acetate ($Co(O\text{-}CO\text{-}CH_3)_2$ 99%, Carlo Erba), respectively. A metal/Al ratio of 1.3 was employed and in order to obtain samples

*e-mail: urquieta@power.ufscar.br

with different Cu and Co contents, the ion exchanges were carried out varying the temperature, the time and the number of exchanges. After each ion exchange, the solids were separated by filtration, washed with deionised water, dried at 110 ºC for 12 h and subsequently activated by heating under air flow at 520 ºC for 1 h, using a heating rate of 10 ºC min^{-1}.

Characterisation

In order to analyse the catalysts with similar chemical characteristics, all samples, prior to be submitted to the different characterisation techniques, they were activated as described above.

The Si/Al ratio of the precursor |Na|[Si_yAl]-**MFI** zeolites was determined using atomic absorption spectroscopy (AAS) and the MFI structure was verified by powder X-ray diffraction (XRD), using a Rigaku Miniflex diffractometer operated with a Cu-K_α radiation and with a goniometer velocity of 2° (2Θ)/min. The morphology of the crystals (size and shape) were determined by scanning electron microscopy (SEM) using a Zeiss DSM 960 microscope operated at 30 kV and with a focus distance between 9 and 14 mm.

The ^{27}Al MAS NMR spectra of the precursor |Na|[Si_yAl]-**MFI** zeolites were obtained on a Varian Unity 400 MHz spectrometer, which worked with a frequency of 104.2 MHz. Aiming to excite only the central transition of the ^{27}Al nuclei, π/16 pulses of 0.4 ms and repetition times of 2 s were used.

The temperature programmed reduction by hydrogen (TPR-H_2) of Cu- and Co-catalysts was carried out using a Micromeritics 2705 equipment having a thermal conductivity detector. It was used a heating rate of 10 ºC min^{-1} and a mixture of 5.1% of H_2 in N_2 (v/v) fed at a flow rate of 30 mL min^{-1}. An amount of 150 mg of sample, previously dried at 110 ºC for 12 h was used in the analysis. To avoid the influence of the physically adsorbed water in the analysis, the samples were previously treated at 200 ºC for 1 h under air flow (30 mL min^{-1}). The water produced during the H_2-TPR was removed through a cold trap.

Raman spectra of Co-catalysts were obtained at room temperature using a radiation of 633 nm from a Ne ion laser that was equipped with a CCD detector. The equipment was operated with a spot size of 1 μm in diameter and a potency that was varied from 70 to 175 μW.

The analysis in the UV/VIS region by diffuse reflectance spectroscopy (DRS) was also performed at room temperature with a Varian Cary 5G spectrometer utilising a Teflon sample holder, a quartz window and a Teflon reference standard. The data obtained were processed by applying the Schuster-Kubelka-Munk function F(R).

Catalytic tests

The activity of the |Cu_x| and |Co_x|[Si_yAl]-**MFI** catalysts was evaluated in the reduction of NO to N_2, using methane or propane as reducing agents, in an oxidative atmosphere. To avoid the formation of hot spots, the catalytic tests were carried out using 50 mg of the catalyst mixed with 150 mg of quartz. The gas mixture (70 mL min^{-1}) was composed of: 0.3% NO, 1.8% O_2, 0.3% C_3H_8 (or 0.3% CH_4) in He (v/v). These operational conditions resulted in a gas hourly space velocity (GHSV) of 42,000 h^{-1}, calculated considering the total gas flow fed to the reactor. The reaction temperature was varied from 150 to 500 ºC.

The products were analysed using a gas chromatograph (Shimadzu-GC-17A) equipped with a flame ionisation detector (FID), a thermal conductivity detector (TCD) and three columns: a capillary (Al_2O_3/KCl, 30 m × 0.32 mm) and two packed columns (Hayesep D (3 m × 1/8″) and Chromossorb 102 (5 m × 1/8″)).

The carbon balance was monitored during the reaction and the activity of the catalysts for the hydrocarbon oxidation was expressed in terms of the total hydrocarbon conversion. The conversion of NO (X_{NO}) was based on the formation of N_2 according to the equation: X_{NO} [%]= 2 [N_2] × 100/[NO]$_0$, where [N_2] = moles of N_2 formed and [NO]$_o$ = moles of NO fed into the reactor.

RESULTS AND DISCUSSION

Precursor characterisation

The XRD patterns of the synthesised |Na|[Si_yAl]-**MFI** zeolites (Figure 1) reveal the presence of the MFI structure that is typical for ZSM-5 zeolites[12]. From Figure 1 it can also be observed for sample |Na|[Si_{45}Al]-**MFI**, the presence of a low intensity peak at 26.64 º(2Θ). This peak corresponds to the reflections related to the α-quartz (101) atomic plane[12].

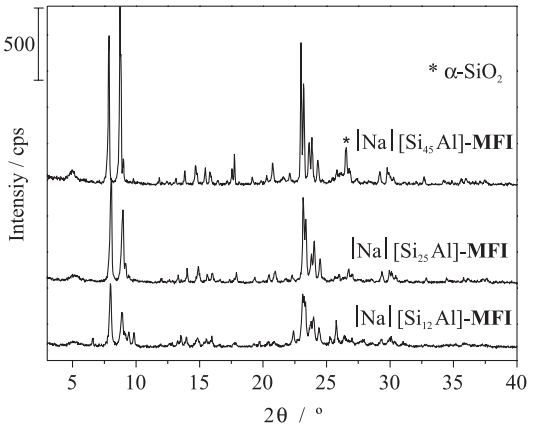

Figure 1. *X-ray diffraction patterns of the activated |Na|[Si_yAl]-**MFI** zeolites*

The Si/Al ratios used in the synthesis gel and those corresponding to the obtained |Na|[Si_yAl]-**MFI** are shown in Table 2. The crystallinity of the samples (Table 2) was calculated from the XRD data (Equation 1) using the |Na|[Si_{45}Al]-**MFI** sample as reference (crystallinity = 100%), since it presented the XRD pattern with the highest peak intensity in the range 22° ≤ 2Θ ≤ 25º.

$$X-ray\ cristallinity\ /\% = \left(\frac{\sum A_{peaks}(22-25^o)_{sample}}{\sum A_{peaks}(22-25^o)_{standard}} \right) \cdot 100 \qquad (1)$$

Although the crystallinities of the |Na|[Si_{12}Al]-**MFI** and |Na|[Si_{25}Al]-**MFI** samples were lower than that of sample |Na|[Si_{45}Al]-**MFI,** neither the XRD patterns nor the SEM micrographs (Figure 2) indicate the presence of amorphous material or other phases. At this point, the reduced intensity of the X-ray reflections may be attributed to the smaller crystal size of these zeolites (see Figures 2a and 2b).

From data given in Table 2 it can be seen that the Si/Al ratios of the synthesised zeolites were lower than those of the correspondent synthesis gels, indicating that aluminium is preferentially incorporated in the zeolite structure[14], and subsequently part of the silica remains as sodium silicate in the liquid phase of the reaction mixture.

Figure 2 shows the SEM micrographs of the |Na|[Si_yAl]-**MFI** zeolites. It can be seen that the aluminium rich zeolite |Na|[Si_{12}Al]-**MFI** (Figure 2a) crystallises foring agglomerates (ca. 15 μm) of small crystals (ca. 3 μm or lower). With the decrease in aluminium content, isolated or twinned hexagonal prisms are formed with dimensions of approximately 20 and 60 μm, as can be seen in the

Table 2. Crystallinity and Si/Al molar ratio in the synthesis gels and in the synthesised zeolites

Sample	X-ray crystallinity (%)	$Si/Al_{reaction\ gel}$	Si/Al_{solid}
|Na|[Si_{12}Al]-MFI	80	15	12
|Na|[Si_{25}Al]-MFI	88	30	25
|Na|[Si_{45}Al]-MFI	100	60	45

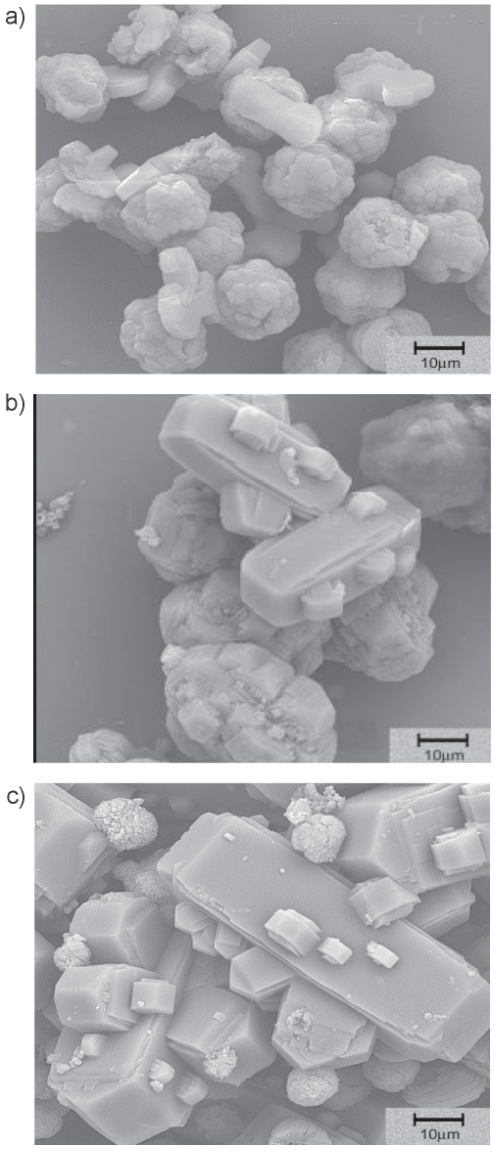

Figure 2. *SEM micrographs of the activated: (a) |Na|[Si_{12}Al]-**MFI**, (b) |Na|[Si_{25}Al]-**MFI** and (c) |Na|[Si_{45}Al]-**MFI***

case of |Na|[Si_{25}Al]-**MFI** and |Na|[Si_{45}Al]-**MFI,** respectively (Figures 2b and 2c). As mentioned above, no amorphous material was observed in the SEM micrographs of the |Na|[Si_{12}Al]-**MFI** and |Na|[Si_{25}Al]-**MFI** (Figures 2a and 2b). On the other hand, Figure 2c shows for |Na|[Si_{45}Al]-**MFI** the presence of small particles (< 1 μm), other than the zeolite crystals. These small particles are probably crystals of α-quartz, which was detected by XRD (Figure 1).

^{27}Al MAS NMR spectra of the |Na|[Si_yAl]-**MFI** zeolites (Figure 3) show a resonance peak at around 53 ppm, which is attributed to tetrahedrally co-ordinated Al atoms that are incorporated into the zeolite framework. For the |Na|[Si_{12}Al]-**MFI** and |Na|[Si_{25}Al]-**MFI** zeolites an additional signal at 0 ppm is observed, which increases with the increase in aluminium content. This signal is associated to the extra-framework octahedrally co-ordinated aluminium, whose phase was not observed by SEM, indicating that it is well dispersed on the external surface or in the micropores of the ZSM-5 crystals. In addition to the lower |Na|[Si_{12}Al]-**MFI** and |Na|[Si_{25}Al]-**MFI** crystal size above commented, the presence of extra-framework aluminium might also explain the lower crystallinity observed by XRD.

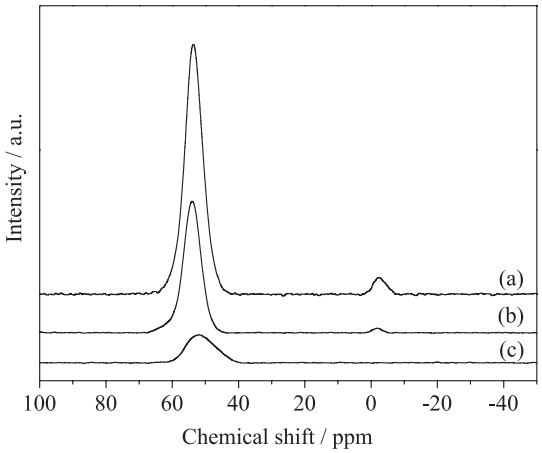

Figure 3. *^{27}Al MAS NMR spectra of the activated: (a) |Na|[Si_{12}Al]-**MFI**, (b) |Na|[Si_{25}Al]-**MFI** and (c) |Na|[Si_{45}Al]-**MFI***

Catalyst characterisation

The elemental composition (Table 3) reveals that in the preparation of Cu-catalysts, the copper content in the samples increases when the exchange temperature is increased from 25 to 50 ºC or when the exchange is repeated. As can also be seen from Table 3, the same tendency is observed for Co-catalysts when the temperature was increased from 25 to 80 ºC.

The TPR-H_2 data for the Cu- and Co-containing catalysts is presented in Figure 4 and Figure 5, respectively, and the observed reduction temperatures and the ratio of consumed H_2 per metal content are showed in Table 4.

As can clearly be observed in Figure 4 and from the data in Table 4 the reduction of |Cu_x|[Si_yAl]-**MFI** catalysts occurs in two well-defined steps, the two peaks having maximum at temperatures between 240 and 305 ºC and between 420 and 600 ºC, respectively. Torre-Abreu *et al.*[15]. attributed the low-temperature peak to the reduction of Cu^{2+} to Cu^+ and the peak at higher temperature to the reduction of Cu^+ to Cu^0. After the TPR analysis, the presence of elemental copper was confirmed by the reddish colour of the samples. Figure 4 and Table 4 also reveal that irrespective of the Si/Al ratio of the zeolite, the reduction temperatures of Cu^{2+} and Cu^+ increase as the copper content decreases. For samples with similar copper content, the reduction temperatures are higher for that with the highest Si/Al ratio. This behaviour might be explained by the lower electronic density of samples with lower aluminium content, which makes the reduction of the metal difficult. Similar trends were observed by Sullivan and Cunningham[16], who attributed such phenomena to an enhanced interaction between the cationic copper species and the zeolite structure. In the TPR-H_2 profiles of samples with higher Cu content, |$Cu_{0.49}$|[Si_{12}Al]-**MFI** and |$Cu_{0.30}$|[Si_{12}Al]-**MFI**, can be observed a small shoulder at around 350 ºC (indicated in Figure 4 with an arrow), which might be attributed to the reduction of finely dispersed CuO particles to elemental Cu^0 [17,18]. As can be seen from Table 4, the sum of H_2/Me ratio corresponding to peak 1 (A1) with the H_2/Me ratio

Table 3. Elemental composition of the prepared $|Cu_x|$ and $|Co_x|[Si_yAl]$-MFI catalysts

Sample	Temperature (ºC)	Exchanges × Exchange time (h)	Metal content (% w/w)	Metal/Al
$|Cu_{0.49}|[Si_{12}Al]$-MFI	25	3 × 12	4.00	0.49
$|Cu_{0.30}|[Si_{12}Al]$-MFI	50	1 × 12	2.41	0.30
$|Cu_{0.18}|[Si_{25}Al]$-MFI	25	2 × 12	0.74	0.18
$|Cu_{0.08}|[Si_{25}Al]$-MFI	25	1 × 12	0.34	0.08
$|Cu_{0.16}|[Si_{45}Al]$-MFI	25	2 × 12	0.36	0.16
$|Co_{0.29}|[Si_{12}Al]$-MFI	80	1 × 48	2.17	0.29
$|Co_{0.58}|[Si_{12}Al]$-MFI	80	3 × 48	4.80	0.58
$|Co_{0.15}|[Si_{25}Al]$-MFI	80	1 × 24	0.59	0.15
$|Co_{0.36}|[Si_{25}Al]$-MFI	80	1 × 48	1.36	0.36
$|Co_{0.01}|[Si_{25}Al]$-MFI	25	1 × 48	0.05	0.01

Table 4. H_2 consumption and peak maximum observed in the TPR-H_2 profiles of $|Cu_x|$ and $|Co_x|[Si_yAl]$-MFI catalysts

Sample	Peak Maximum (ºC)			H_2/Me (A1) [a]	H_2/Me (A2) [a]	H_2/Me (A3) [a]	H_2/Me Total [a]
	1st	2nd	3rd				
$|Cu_{0.49}|[Si_{12}Al]$-MFI	240	420	-	0.49	0.49	-	1.07
$|Cu_{0.30}|[Si_{12}Al]$-MFI	250	450	-	0.46	0.45	-	0.98
$|Cu_{0.18}|[Si_{25}Al]$-MFI	245	615	-	0.49	0.43	-	0.92
$|Cu_{0.16}|[Si_{25}Al]$-MFI	270	630	-	0.56	0.52	-	1.08
$|Cu_{0.08}|[Si_{45}Al]$-MFI	305	600	-	0.52	0.47	-	0.99
$|Co_{0.58}|[Si_{12}Al]$-MFI	320	-	750	0.10 (0.06) [b]	-	1.22	1.32
$|Co_{0.36}|[Si_{25}Al]$-MFI	-	-	780	-	-	0.95	0.95
$|Co_{0.29}|[Si_{25}Al]$-MFI	-	-	770	-	-	1.15	1.15

[a] moles of consumed H_2 / moles of Cu^{2+} or Co^{2+}. [b] in brackets is indicated the ratio of consumed H_2 / moles of Co^{3+}.

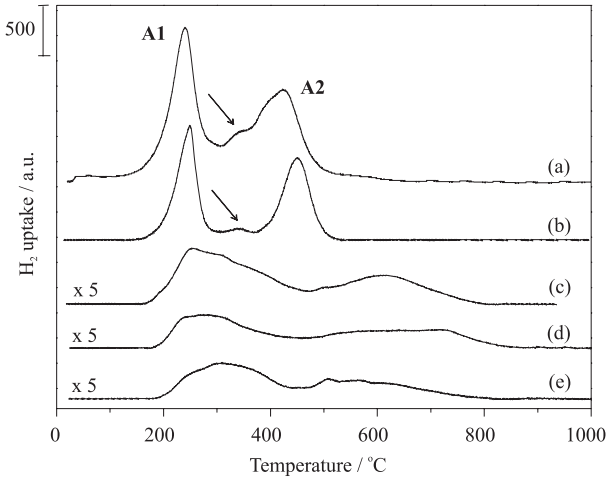

Figure 4. *TPR-H_2 profiles of the activated: (a) $|Cu_{0.49}|[Si_{12}Al]$-**MFI**, (b) $|Cu_{0.30}|[Si_{12}Al]$-**MFI**, (c) $|Cu_{0.18}|[Si_{25}Al]$-**MFI**, (d) $|Cu_{0.16}|[Si_{45}Al]$-**MFI** and (e) $|Cu_{0.08}|[Si_{25}Al]$-**MFI***

corresponding to peak 2 (A2) does not correspond to the total hydrogen consumption (H_2/Me total). This difference in the H_2 consumption might be attributed to the presence of CuO, whose content in each catalyst (show in Table 5) was estimated considering the stoichiometry of the CuO reduction: $CuO + H_2 \rightarrow Cu^0 + H_2O$; resulting in 0.4 and 0.17% w/w for the $|Cu_{0.49}|$ and $|Cu_{0.30}|[Si_{12}Al]$-**MFI**, respectively.

CuO can be formed during calcination from hydroxylated species generated during the ion exchange[19], such as $Cu^{n+}(OH)_n$, $Cu^{(n+m)+}(OH)_m(O\text{-}CO\text{-}CH_3)_n$ or $Cu^{n+}(OH)_m{}^{(n-m)+}$, resulting in a pH decrease from 5.5 to 4.9.

As can be seen from the TPR-H_2 profiles of Figure 5, all the $|Co_x|[Si_yAl]$-**MFI** catalysts show an intense reduction peak with maximum at temperatures between 660 and 720 ºC (Table 4). Wang *et al.*[20]. and Cruz *et al.*[21]. attributed this peak to the reduction of Co^{2+} to Coº in charge- compensating sites of the zeolite structure. For the $|Co_{0.58}|[Si_{12}Al]$-**MFI** catalyst, which has the highest cobalt content, the low intensity reduction peak at around 320 ºC, might be attributed to the reduction of cobalt oxide species. As in the case of CuO, the Co_3O_4 content in the Co-catalysts (Table 5) was estimated from the stoichiometry of its reduction, using the consumed H_2 (peak at 320 ºC), resulting for the $|Co_{0.58}|[Si_{12}Al]$-**MFI** in 0.7% w/w. In the other samples this peak was not observed, probably due to their lower cobalt content. As in the case of Cu-catalysts, the formation of cobalt oxides is also related to the formation of cobalt hydroxide species during ion exchange, where a pH decrease from 6.0 to 4.9 was observed.

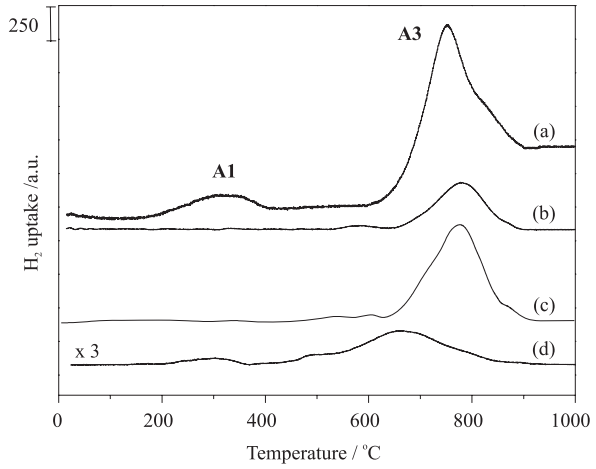

Figure 5. *TPR-H_2 profiles of the activated: (a) $|Co_{0.58}|[Si_{12}Al]$-**MFI**, (b) $|Co_{0.36}|[Si_{25}Al]$-**MFI**, (c) $|Co_{0.29}|[Si_{12}Al]$-**MFI** and (d) $|Co_{0.15}|[Si_{25}Al]$-**MFI***

As mentioned, Table 4 also presents the ratio of total consumed H_2 per metal content for Cu and Co-catalysts. Theoretically, for each divalent metal cation (Me^{2+}) reduced to Me^0 the H_2/Me ratio should be equal to 1. H_2/Me values below 1 could indicate incomplete reduction of the metal, while values higher than 1 could be related to the simultaneous reduction of species other than the Me^{2+} cations. For Cu-catalysts no significant deviation from 1 is observed, indicating complete reduction of copper species. For the sample $|Co_{0.58}|[Si_{12}Al]$-**MFI** a value of H_2/Me equal to 1.32 was obtained, which can be explained by considering the simultaneous reduction of Co^{2+} and trivalent Co^{3+}. The trivalent species are present due to the partial oxidation of Co^{2+} (present in CoO) to give Co^{3+} and generating Co_3O_4. Similar observations were made by Wang *et al.*[20] for cobalt-containing ZSM-5 zeolite.

In order to obtain further information about the Co-oxide species present in the Co-catalysts, Raman measurements were performed. Figure 6 shows the spectra obtained from the $|Co_{0.58}|[Si_{12}Al]$-**MFI** catalyst, Co_3O_4 (reference sample) and the zeolite used as precursor. As can be seen, the bands at 303 and 385 cm^{-1} in the spectrum of $|Co_{0.58}|[Si_{12}Al]$-**MFI** correspond to the zeolite framework and they are not related to the Co-species[22]. In addition, bands at 197, 483, 529, 616 and 692 cm^{-1} can be observed in the spectra. These bands are attributed to Co_3O_4 agglomerates, which must be smaller than 3 nm, as they were not detected by XRD. In the same spectrum, a band at around 580 cm^{-1} is also observed. As this band can not be attributed to the zeolite framework nor to Co_3O_4, it is suggested that it corresponds to a loaded cobalt species other than Co_3O_4 (*e. g.* CoO(OH))[22].

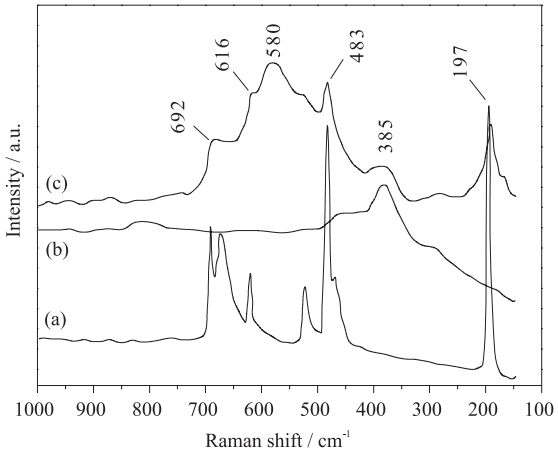

Figure 6. *Raman spectra of the activated: (a) Co_3O_4, (b) $|Na_x|[Si_{12}Al]$-**MFI** and (c) $|Co_{0.58}|[Si_{12}Al]$-**MFI***

Figure 7 shows the DRS-UV/VIS spectra of the $|Cu_x|[Si_yAl]$-**MFI** catalysts. The presence of bands at around 212, 256 and a broad, but weak band between 600 and 850 nm can be observed. Itho *et al.*[23] reported that the band at 212 nm, which appears in the spectra of all samples, is related to the zeolitic support and therefore not related to the Cu-species. The band at 256 nm is attributed to Cu^{2+} interacting with oxygen atoms in the zeolite structure and the band between 600 and 850 nm to Cu^{2+} cations in hexagonal coordination (this band is indicated in Figure 7 between arrows)[23,24]. Although the above discussed TPR-H_2 results suggest the presence of small amounts of CuO in the $|Cu_x|[Si_yAl]$-**MFI** catalysts, in their DRS-UV/VIS spectra there is no band at around 890 nm, which could indicate the presence of this species[25]. This fact could be a consequence of the low concentration of CuO in the samples.

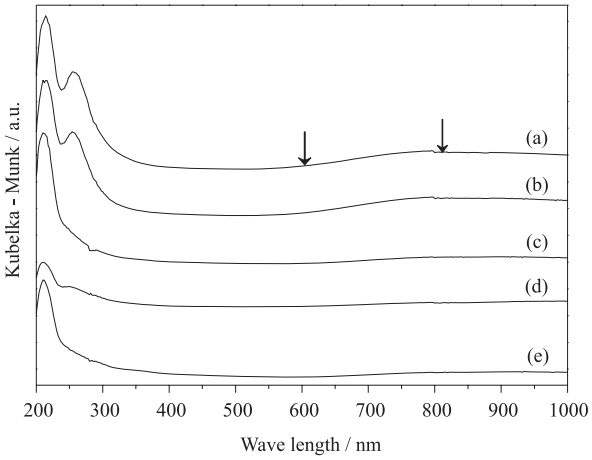

Figure 7. *DRS-UV/Vis spectra of the activated: (a) $|Cu_{0.49}|[Si_{12}Al]$-**MFI**, (b) $|Cu_{0.30}|[Si_{12}Al]$-**MFI**, (c) $|Cu_{0.18}|[Si_{25}Al]$-**MFI**, (d) $|Cu_{0.16}|[Si_{45}Al]$-**MFI** and (e) $|Cu_{0.08}|[Si_{25}Al]$-**MFI***

In the DRS-UV/VIS spectra of $|Co_x|[Si_yAl]$-**MFI** catalysts bands at 210, 255 and between 415 – 600 nm can be observed (Figure 8). The latter, which is present only in samples with a high metal content, is attributed to Co_3O_4 oxide[26]. The bands at 210 and 255 nm are associated to the electronic transitions of the zeolite structure and to Co^{2+} species compensating the negative charge of the zeolite, respectively.

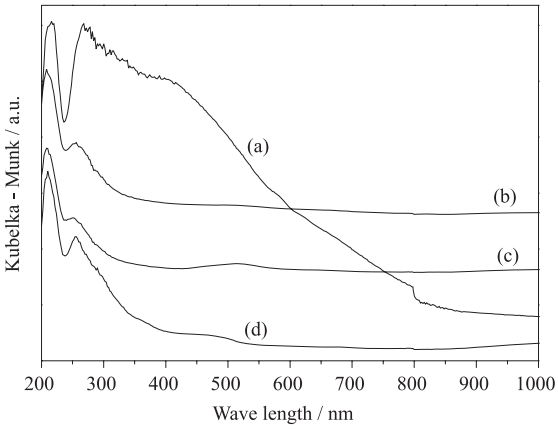

Figure 8. *DRS-UV/Vis spectra of the activated: (a) $|Co_{0.58}|[Si_{12}Al]$-**MFI**, (b) $|Co_{0.36}|[Si_{25}Al]$-**MFI**, (c) $|Co_{0.29}|[Si_{12}Al]$-**MFI** and (d) $|Co_{0.15}|[Si_{25}Al]$-**MFI***

In the activated $|Co_{0.58}|[Si_{12}Al]$-**MFI** sample, these bands are broader and more intense, particularly the band at 415 – 600 nm. Therefore, in this catalyst, Co^{3+} species are probably present in a higher proportion, thus explaining its higher H_2/Co ratio obtained in the TPR (see Table 4) and the Co_3O_4 bands detected by Raman spectroscopy.

Catalytic evaluation

In the following discussion about the activity of the Cu- and Co-catalysts, it was not considered the effect of water generated in the hydrocarbon oxidation. As mentioned, the amount of water formed (lower than 0.6% v/v) is not plausible to cause appreciable deactivation[7].

Figure 9a shows the conversion of NO to N_2 on $|Cu_x|[Si_yAl]$-**MFI** as a function of the reaction temperature, using propane or

methane as reducing agent. It can be observed that the conversion of NO depends on the temperature, the type of hydrocarbon and the copper content.

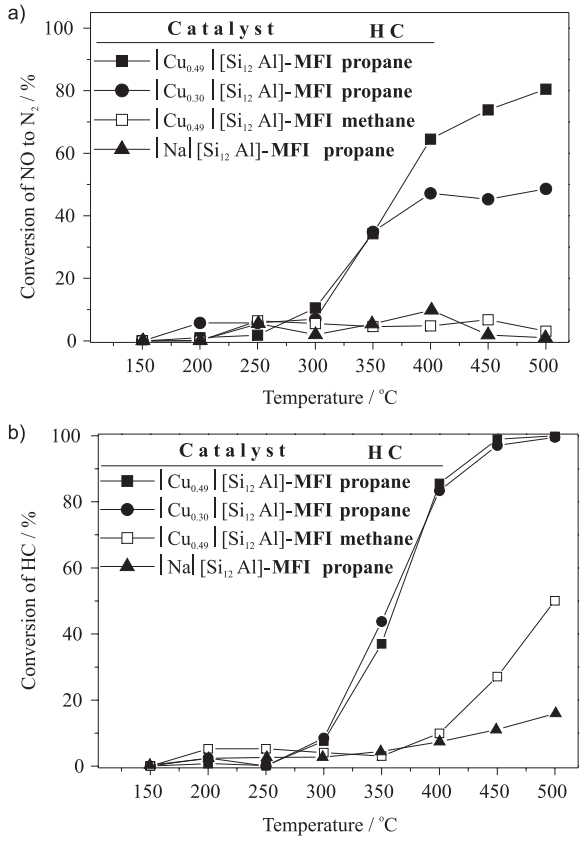

Figure 9. *Conversion of: (a) NO to N_2 and (b) hydrocarbon, as a function of the temperature for the activated $|Cu_x|[Si_yAl]$-**MFI** catalysts*

The $|Cu_x|[Si_{12}Al]$-**MFI** catalysts, in comparison with the precursor $|Na|[Si_{12}Al]$-**MFI** zeolite (Figure 9), are active catalysts for the conversion of NO to N_2 in the presence of propane and their activity increases as the copper content increases. For propane oxidation, the activity of the studied $|Cu_x|[Si_yAl]$-**MFI** catalysts was not influenced by the metal content and it was only slightly modified in the presence or in the absence of NO (Figure 10). When NO was fed to the reactor, the propane conversion decreased due to the competition between propane and NO for the active sites of the catalyst (Table 1, reactions 1 and 2). On the other hand, Figure 9 reveals that $|Cu_x|[Si_yAl]$-**MFI** catalysts are not active in the reduction of NO in the presence of methane and also show low activity in the oxidation of this hydrocarbon. This behaviour was also observed by Li and Armor[27] and it is probably related to the high energy necessary for the C-H dissociation in methane, which is following Adelman *et al.*[28], the limiting step in the reduction of NO by alkanes over copper-containing ZSM-5 zeolites. For the $|Cu_x|[Si_yAl]$-**MFI** catalysts in the tests using propane, it can be seen that the conversion of NO increases more slightly at temperatures higher than 400 ºC. This behaviour is attributed to an increase in the desorption rate of NO at higher temperatures and to a decrease in the propane concentration, which is associated with the increase of its direct oxidation by O_2 at those temperatures (Table 1, reaction 2).

Figure 11 shows that $|Co_x|[Si_yAl]$-**MFI** catalysts have low activity for the reduction of NO to N_2 in the presence of propane. On the other hand, in the presence of methane, which is also partially converted, $|Co_x|[Si_yAl]$-**MFI** catalysts reduce in more extension NO to N_2 (Table 1, reaction 3), with the conversion increasing with the increase in the cobalt content in the catalyst. This behaviour, which differs from that obtained on $|Cu_x|[Si_yAl]$-**MFI** catalysts using the same hydrocarbon, might be explained by the different intermediate nitrogen species formed on each catalyst. Adelman *et al.*[28] found that in the presence of NO and O_2, nitro and/or nitrate complexes ($[Cu(NO_2)_y]^{2+}$ or $Cu[(NO_3)_y]^{(2-y)+}$) are predominantly formed on $|Cu_x|[Si_yAl]$-**MFI**, while nitrite complexes ($[Co(ONO)_y]^{2+}$) are predominant on $|Co_x|[Si_yAl]$-**MFI** catalysts. The latter are reduced

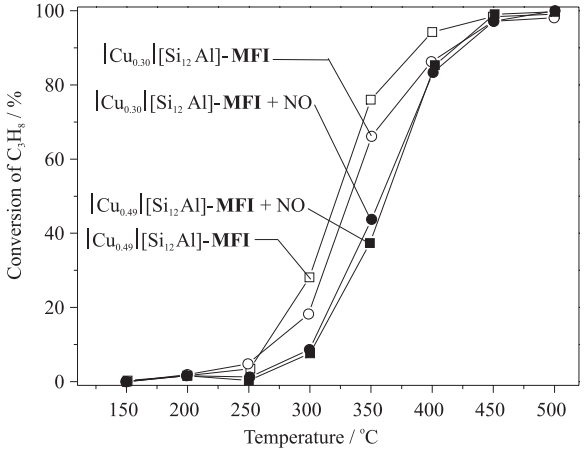

Figure 10. *Propane oxidation on activated $|Cu_x|[Si_{12}Al]$-**MFI** catalysts, in the presence or in the absence of NO*

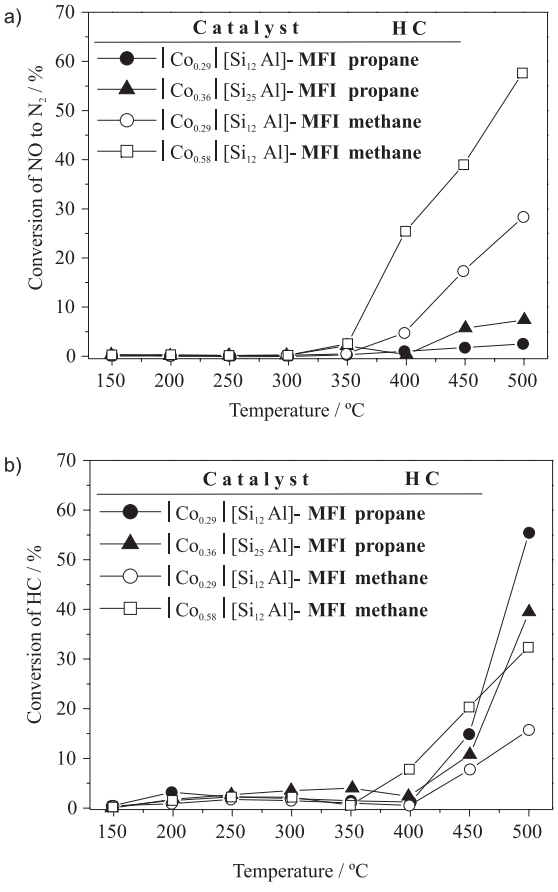

Figure 11. *Conversion of: (a) NO to N_2 and (b) hydrocarbon as function of the temperature for the activated $|Co_x|[Si_yAl]$-**MFI** catalysts*

upon exposure to CH_4 leading to the formation of N_2 and different methane oxidation products, while the nitro and/or nitrate complexes are chemically reduced to N_2 upon exposure to C_3H_8 and remain inert in the presence of CH_4.

Figure 12 shows the conversion of propane on $|Co_x|[Si_yAl]$-**MFI** catalysts with different cobalt contents. As can be observed, these catalysts show similar behaviour that was observed for the copper-containing catalysts, in which the conversion of propane was decreased due to the competition between NO and propane for the active sites.

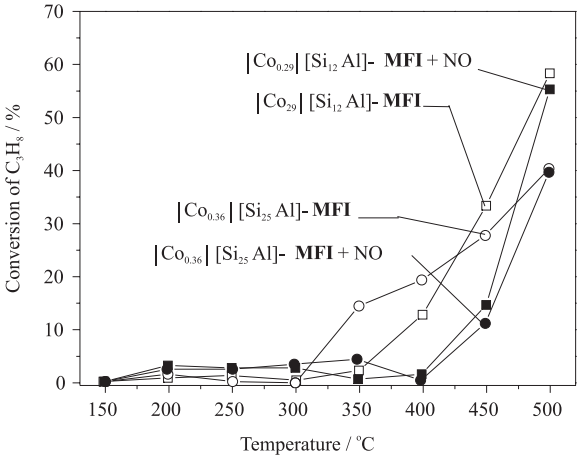

Figure 12. *Propane oxidation on activated $|Co_x|[Si_yAl]$-**MFI** catalysts, in the presence or in the absence of NO*

The analysis of the reaction products by gas chromatography demonstrated that the oxidation of propane on copper-catalysts was more selective towards the formation of CO_2. For propane and methane oxidation on cobalt-catalysts, in addition to CO_2, partially oxidised hydrocarbons, such as aldehydes and ketones, were also observed.

Considering the total metal content in the studied catalysts (Table 3), Table 5 shows the observed specific activity during the reduction of NO to N_2 on $|Cu_x|$ and $|Co_x|[Si_yAl]$-**MFI**. As can be seen, the higher the Cu loading in the in the former catalysts the lower their specific activity. This behaviour might be attributed to the different metal content in the catalytic bed and to the different nature of the Cu^{2+} cations as was commented during the discussion of the TPR-H_2 analyses. On the other hand, for a higher metal content in the Co-catalysts a slightly higher specific activity is observed. As can also be seen in Table 5, the amount of metallic oxide present in the samples increases with the metal content. The specific activity and TPR-H_2 data of Cu-catalysts can indicate that CuO species are practically not active, however Co_3O_4 species seem to favour the activity of Co-catalysts.

Table 5. Specific activity and metal oxide content observed for the $|Cu_x|$ and $|Co_x|[Si_yAl]$-MFI catalysts

	Specific Activity (mols of N_2 formed).(mols of metal)$^{-1}$. h^{-1}		
Sample	450 ºC	500 ºC	% M_xO_Y [c]
$|Cu_{0.30}|[Si_{12}Al]$-MFI [a]	8.3	9.4	0.17
$|Cu_{0.49}|[Si_{12}Al]$-MFI [a]	7.5	7.8	0.4
$|Co_{0.29}|[Si_{12}Al]$-MFI [b]	3.5	5.6	0
$|Co_{0.58}|[Si_{12}Al]$-MFI [b]	4.1	5.9	0.7

In the presence of: [a] propane and [b] methane.[c] Estimated massic percentage, considering CuO (Cu-catalysts) and Co_3O_4 (Co-catalysts). The values were obtained from TPR data as is indicated in the text.

CONCLUSIONS

The synthesised |Na|-zeolites presented **MFI** structure and it was observed that with the decrease in aluminium content their morphology changed from aggregates of small crystals to isolated or twinned hexagonal prisms. The species present in $|Cu_x|$ and $|Co_x|[Si_yAl]$-**MFI** catalysts were mostly Cu^{2+} and Co^{2+} cations, which are compensating the negative charge of the zeolite structure. In the catalysts with higher metal content it was also evidenced the presence of metal oxides, generated during the calcination of $Me(OH)_2$, $Me^{2+}(OH)^-$ or $Me(O\text{-}CO\text{-}CH_3)_2$ species, which are formed during ion exchange.

In the reduction of NO the activity of the catalysts increased as the content of the charge-compensating Cu^{2+} and Co^{2+} species increased. $|Cu_x|[Si_yAl]$-**MFI** catalysts were only active in the presence of propane and they showed higher activity at lower temperatures than the $|Co_x|[Si_yAl]$-**MFI** catalysts, the latter being more active with methane.

It the oxidation of hydrocarbons the Co-based catalysts were less selective for the formation of CO_2. For both type of studied catalysts it was verified that in detriment to the desired oxidation with NO, occurs preferentially their oxidation with O_2.

REFERENCES

1. Pârvulescu, V. I.; Grange, P.; Delmon, B.; *Catal. Today* **1998**, *46*, 233.
2. Rangel, M. C.; Carvalho, M. F. A.; *Quim. Nova* **2003**, *26*, 265.
3. Amiridis, M. D.; Zhang, T.; Farrauto, R. J.; *Appl. Catal., B* **1996**, *10*, 203.
4. Iwamoto, M.; Hamada, H.; *Catal. Today* **1991**, *10*, 57.
5. Beutel, T.; Sarkany, J.; Lei, G. D.; Yan, J. Y.; Sachtler, W. M. H.; *J. Phys. Chem.* **1996**, *100*, 845.
6. Gómez, S. A.; Campero, A.; Marínez-Hermández, A.; Fuentes, G. A.; *Appl. Catal., A* **2000**, *197*, 157.
7. Tabata, T.; Kokitsu, M.; Okada, H.; Sabatino, L. M. F.; *Catal. Today* **1996**, *27*, 91.
8. Li, Y; Battavio, P. J.; Armor, J. N.; *J. Catal.* **1993**, *142*, 561.
9. Batista, M. S.; *Ph. D. Thesis*, Universidade Federal de São Carlos, Brasil, 2002.
10. Atkins, P.; Jones, L.; *Chemical Principles*, 2nd ed., W. H. Freeman and Company: New York, 2001.
11. McCusker, L. B.; Liebau, F.; Engelhardt, G.; *Pure Appl. Chem.* **2001**, *73*, 381.
12. Treacy, M. M. J.; Higgins, J. B.; von Ballmoos, R.; *Zeolites* **1996**, *16*, 327.
13. Batista, M. S.; *Master Thesis*, Universidade Federal de São Carlos, Brasil, 1997.
14. Jahn, S. L.; *Ph. D. Thesis*, Universidade Federal de São Carlos, Brasil, 1987.
15. Torre-Abreu, T. C.; Henriques, C.; Ribeiro, F. R.; Delahay, G.; Ribeiro, M. F.; *Catal. Today* **1999**, *54*, 407.
16. Sullivan, J. A.; Cunningham, J.; *Appl. Catal., B* **1998**, *15*, 275.
17. Carniti, P.; Gervasini, A.; Modica, V. H.; Ravasio, N.; *Appl. Catal., B* **2000**, *28*, 175.
18. Minchev, C.; Köhn, R.; Tsonsheva, T.; Dimitrov, M.; Fröba, M.; *Stud. Surf. Sci. Catal.* **2001**, *135*, 253.
19. Martins, L.; Peguin, R. P. S.; Wallau, M.; Urquieta-González, E. A.; *J. Braz. Chem. Soc.* **2005**, *16*, 589.
20. Wang, X.; Chen, H. Y.; Sachtler, W. M. H.; *Appl. Catal., B* **2000**, *26*, L227.
21. Cruz, R. S. da; Mascarenhas, A J. S.; Andrade, H. M. C.; *Appl. Catal., B* **1998**, *18*, 223.
22. Ohtsuka, H.; Tabata, T.; Okada, O.; Sabatino, L. M. F.; Belusi, G.; *Catal. Today* **1998**, *42*, 45.
23. Itho, Y.; Nishiyama, S.; Tsuruya, S.; Masai, M.; *J. Phys. Chem.* **1994**, *98*, 960.
24. Moretti, G.; Dossi, C.; Fusi, A.; Recchia, S.; Psaro, R.; *Appl. Catal., B* **1999**, *20*, 67.
25. Dossi, C.; Fusi, A.; Recchia, S.; Psaro, R.; Moretti, G.; *Microporous Mesoporous Mater.* **1999**, *30*, 165.
26. Fierro, G.; Eberhardt, M. A.; Houalla, M.; Hercules, D. M.; Hall, W. K.; *J. Phys. Chem.* **1996**, *100*, 8468.
27. Li, Y.; Amor, J. N.; *Appl. Catal., B* **1993**, *2*, 239.
28. Adelman, B. J.; Beutel, T.; Lei, G. D.; Sachtler, W. M. H.; *J. Catal.* **1996**, *158*, 327.